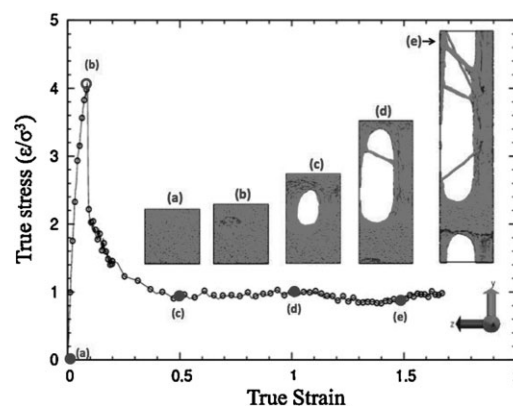


# Predictors of Cavitation in Glassy Polymers under Tensile Strain: A Coarse-Grained Molecular Dynamics Investigation

Ali Makke,\* Michel Perez, Jörg Rottler, Olivier Lame, Jean-Louis Barrat

The nucleation of cavities in a homogeneous polymer under tensile strain is studied in a coarse-grained MD simulation. To establish a causal relation between local microstructure and the onset of cavitation, a detailed analysis of some local properties is presented. In contrast to common assumptions, the nucleation of a cavity is neither correlated to a local loss of density nor to stress at the atomic scale or the chain-end density in the nondeformed state. Instead, a cavity in glassy polymers nucleates in regions that display a low bulk elastic modulus. Even if the localization of a cavity is not directly predictable from the initial configuration, the elastically weak zones identified in the initial state emerge as favorite spots for cavity formation.



## Introduction

Under hydrostatic stress conditions, failure of amorphous polymers occurs through cavitation, often followed by crazing, i.e., the formation of interpenetrating microvoids.<sup>[1]</sup> Similarly, the plastic deformation of semi-crystalline polymers is strongly correlated to the nucleation of cavities in the amorphous region.<sup>[2]</sup> Although essential to control deformation and failure of many organic materials, cavitation in glassy polymers under load is poorly understood. To our knowledge, the microstructural causes, or the

precursors of cavitation at a microscopic scale, are not clearly identified. Although it is known that impurities or surface defects aid the nucleation of cavities,<sup>[3,4]</sup> it is presently not possible to predict where cavitation will take place in the polymer.

Classical nucleation theory, where elastic energy is balanced by the creation of free surface, was used by Argon and Hannoosh to model the cavitation nucleation.<sup>[4]</sup> Estevez et al. investigated the fracture toughness in glassy polymers using mechanical approaches with empirical constitutive equations to describe the competition between shear yielding and crazing.<sup>[5]</sup> They noted that the development of crazes is favored by a fast local deformation.

According to Gent,<sup>[6]</sup> crazing in glassy plastics can be attributed to a local stress-activated devitrification. It is generally agreed that large triaxial tensile stresses are needed to induce cavitation, which forms the basis of several macroscopic craze initiation and cavitation criteria.<sup>[7,8]</sup> Molecular dynamics (MD) simulations of polymer glasses also found a transition from shear yielding, which obeys a pressure-modified von Mises yield criterion,<sup>[9]</sup> to cavitation as the hydrostatic pressure

A. Makke, J.-L. Barrat  
Université Lyon I, LPMCN-UMR CNRS 5586, F69622 Villeurbanne,  
France

E-mail: ali.makke@insa-lyon.fr

A. Makke, M. Perez, O. Lame  
Université de Lyon, INSA Lyon, MATEIS-UMR CNRS 5510, F69621  
Villeurbanne, France

J. Rottler  
Department of Physics and Astronomy, University of British  
Columbia, 6224 Agricultural Road, Vancouver, BC, V6T 1Z1, Canada

becomes negative, but have not yet investigated the connection between cavitation and local microstructural configuration. More recent simulations explored correlations between the location of failure and regions of higher mobility or higher chain ends density that might act as local defects,<sup>[10]</sup> or a local stress-induced disentanglement of chains.<sup>[11]</sup> In the latter work a primitive path algorithm was used to monitor the entanglement network in a sample undergoing triaxial deformation, and it was found that regions undergoing crazing were also depleted in terms of entanglements.

The local mechanical properties are a determining factor to understand the response of systems under strain. Yoshimoto et al.<sup>[12,13]</sup> have calculated the local elastic modulus in a coarse grained polymer glass using a thermodynamic approach based on stress fluctuation. They found that polymers are mechanically heterogeneous at local scale. Papakonstantopoulos et al.<sup>[14]</sup> have studied the earliest local plastic events observed in the elastic regime of polymer glass. They found that these irreversible events take place in domains that exhibit a low positive elastic modulus. Analogous results were obtained by Tsamados et al. on Lennard-Jones glasses submitted to a quasistatic shear strain.<sup>[15]</sup> They found a correlation between high non-affine displacements (NADs) and local low elastic modulus. It is unclear, however, if these criteria can be used in a predictive manner, in the sense that the cavitation event could be predicted from the configuration of an unstrained system.

In this paper, we therefore investigate the correlation between the microstructure of a homopolymer at the segmental level and the nucleation of cavities with molecular dynamics simulations, in an attempt to find a microstructural *predictor* of such events. The Section 'Methods' will present technical details of the simulations and will demonstrate that the non-affine particle displacement is a particularly suitable tool for characterizing and locating cavities. The Section 'Microstructural Causes and Precursors of Cavitation' is devoted to the investigation of possible causes of cavitation, namely (i) local excess of free volume, (ii) local excess of atomic stress, (iii) local density of beads and chain ends, and (iv) local bulk modulus. We will show that while (i)–(iii) bear little correlation to the NAD, the local bulk modulus (iv) has a much better potential to predict the cavitation event.

## Methods

### MD Simulations

MD simulations were carried out for a well-established coarse-grained model, in which the polymer is treated as a

linear chain of  $N$  beads of mass  $m$ , which we refer to as monomers, connected by stiff anharmonic springs that prevent chain crossing and breaking.<sup>[16]</sup> The beads interact through a conventional 6–12 Lennard-Jones potential that is truncated at 2.5 times the particle diameter (The tiny discontinuity of the force at the cutoff distance, less than 1% of the maximal attractive part, has no consequence). All quantities will be reported in units of the Lennard-Jones length scale  $\sigma$  and energy scale  $\epsilon$ , and the characteristic time is  $\tau_{\text{LJ}} = \sqrt{m\sigma^2/\epsilon}$ . Newton's equations of motion are integrated with the velocity Verlet method and a time step  $\Delta t = 0.006$ . Periodic simulation cells of initial size  $L_x(0) = L_y(0) = L_z(0) = 34.2$  containing  $M = 215$  chains of size  $N = 200$  beads were used with a Nosé-Hoover thermostat, i.e., in the *NVT* ensemble. All samples were generated using the "radical-like" polymerization method.<sup>[17]</sup> The polymerization starts from a Lennard-Jones liquid, where 215 beads are chosen randomly to behave as "radical" sites. Each radical bead is allowed to connect to a free and nearest neighbor with a strong covalent bond. The radical sites are then transferred to the new connected beads, allowing thus the growth of all chains. If no monomers are near the radical, no finitely extensible nonlinear elastic (FENE) bond is created. Another attempt will be performed at the next growth stage. Between two growth stages, the entire system is relaxed during 100 MD steps. The polymerization propagates until all chains reach their target length of 200 beads. When the generation is terminated, residual single beads are removed and the system is relaxed for  $10^7$  MD steps in the *NPT* ensemble at  $T = 1$  and  $P = 0$  to reach an equilibrium state. The equilibration leads to a "mean square internal distance" very close to the function given by Auhl et al.<sup>[18]</sup> The polymer is then rapidly quenched into the glassy state at a temperature  $T = 0.2$  in the *NPT* ensemble (cooling rate:  $1\epsilon$  per  $10^6$  MD steps). The glass transition temperature is  $T_g = 0.43^a$ . The pressure remains zero and the sample density reaches 1.04 before applying the deformation.

Triaxial tensile test conditions were employed.<sup>[19]</sup> The samples were subjected to a sequence of deformation-relaxation steps, composed of (i) a rescaling of the simulation box in the tensile direction  $\{y$  in our case so that the true strain is  $\epsilon_{yy}(t) = \ln[L_y(t)/L_y(0)]$ , whereas the two other dimensions remain unchanged, followed by (ii) an MD step in the *NVT* ensemble. The deformation rate was chosen to be  $\dot{L}_y = 0.0025$ , so that the initial strain rate is  $\dot{\epsilon}_{yy}(0) = 7.3 \times 10^{-5}$ . Over the range of strain investigated, the true strain rate remains essentially constant. Note that the applied deformation trajectory leads to a high level of triaxiality, which is the basic

<sup>a</sup>  $T_g^*$  has been determined by the slope change observed when the sample volume is plotted with respect to the temperature during cooling from  $T = 1$  to 0.0001 under *NPT* conditions.

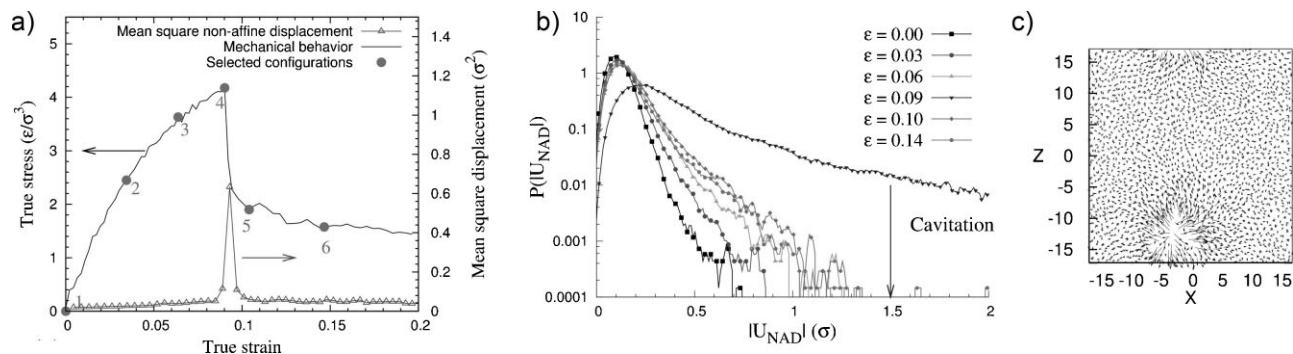


**Figure 1.** (a) Stress/strain curve of a glassy polymer at  $T=0.2$  during a triaxial tensile test. A peak in the mean square NAD is observed simultaneously with the drop of the stress due to cavitation. Markers 1–4 indicate the selected configurations for which distributions of NAD are plotted in (b). These distributions show an exponential tail for configuration 4, due to the large amplitude motions caused by cavitation. (c) Representation of the NAD in a cross-section of the sample containing the cavity, for configuration 4.

ingredient for cavitation. As the deformation proceeds, configurations were recorded along the trajectory in order to analyze their microstructure.

### Non-Affine Displacement: A Tool for Characterizing Cavitation

The mechanical behavior of our glassy polymers under triaxial tensile conditions is illustrated in Figure 1(a). Three main regimes can be distinguished: (i) elastic, (ii) viscoelastic, and (ii) drawing regime, which occurs at constant stress. In the elastic regime, the increase of deformation will slightly shift the bead positions from their local energy minima, resulting in reversible behavior. This regime is limited to a very low strain 0.001 as demonstrated by Schnell.<sup>[20]</sup> In the viscoelastic regime, stress is relaxed by inter-chain sliding. This stage is limited by a strong drop of stress. When a critical deformation is reached, cavities will nucleate and then part of the stored elastic energy is released as free surfaces open up. Note that the strain hardening regime is not shown in Figure 1(a), since it occurs at larger strains when the entanglement network of chains and fibrils becomes stretched.<sup>[9]</sup>

The detection of cavity nucleation could be performed visually on snapshots that are regularly stored during the course of the tensile test. However, small cavities in a three dimensional sample can be delicate to observe. Therefore, a more versatile indicator is needed. The NAD is the perfect candidate for such observation and has been successfully used to monitor local plastic activity in 2D amorphous Lennard-Jones packings under athermal quasistatic deformation.<sup>[21]</sup> Note that NAD fluctuations cannot find their origin in the thermal motion of atoms since, in the framework of this paper, specimens are maintained well below their glass transition temperature ( $T = 0.2 < T_g = 0.43$ ). Moreover, the NAD

can be used as a routine tool and it starts to increase locally, in the early stages of cavity nucleation, even before the cavity could be observed visually on a snapshot of the sample.

The NAD ( $\mathbf{u}_{na}^i$ ) is defined as the difference between the displacement ( $\mathbf{r}^i(t + \delta t) - \mathbf{r}^i(t)$ ) and the displacement it would experience if the deformation were perfectly affine, i.e., homogeneous at all scales,

$$\mathbf{u}_{na}^i(t) = \mathbf{r}^i(t + \delta t) - \mathbf{r}^i(t) - \dot{\epsilon}_{yy}(t) \delta t r_y^i(t) \mathbf{e}_y \quad (1)$$

where  $\mathbf{r}^i(t)$  is the position of bead  $i$  at time  $t$ ,  $r_y^i(t)$  the projection of this position along the  $y$  axis, and  $\delta t$  is the time elapsed between two configurations where the NAD is evaluated (typically  $30\tau$ ).

In Figure 1(a), the cavity nucleates at  $\epsilon_{yy} = 0.09$ . At the same strain, the NAD exhibits a peak. Beads that exhibit the largest NAD are those which belong to the surface of the cavity [see Figure 1(c)]. Figure 1(b) shows the evolution of the NAD distribution for several deformations. Before cavitation, increasing the deformation shifts the distribution tail to larger NAD until the very moment at which the growth of a cavity occurs, which is associated with very large values of NAD [see Figure 1(c)]. A threshold for NAD magnitude has been defined: if  $|\mathbf{u}_{na}^i| > 1.5\sigma$  at the yielding point, the bead  $i$  is said to belong to the cavity surface. This threshold is used to identify the “cavity beads” in order to follow some of their local properties. The position of the cavity is defined as the center of mass of these “cavity beads.” After cavitation, the distribution returns to a narrower shape. Note that the NAD distribution broadens even before the stress drop in the stress/strain curve, due to the nucleation of the cavity. In the following sections, NAD will be used as a quantitative tool for investigating the possible correlations with other microstructural or mechanical properties,

such as Voronoi volume, hydrostatic stress, local density, and local moduli.

## Microstructural Causes and Precursors of Cavitation

In this section, we will attempt to correlate NAD fluctuations with some local properties measured at the scale of a single “atom” (Voronoi volume and stress per atom), and properties averaged on the scale of a few particle diameters (chain end density and bulk modulus).

### Voronoi Volume Fluctuations

The concept of free volume has been extensively used to explain many specific properties of supercooled liquids and glasses. Free volume is defined as the volume in excess compared to an ideal disordered atomic configuration of maximum density. One of the simplest ways to compute free volume on a local scale (and to avoid the ambiguity of the above definition) is the Voronoi tessellation, which uniquely assigns a polygonal volume to each bead, formed by intersecting the planes bisecting the lines between different bead centers. In order to determine whether local fluctuations of free volume (or Voronoi volume) favor the nucleation of a cavity, we used the `voro ++` routine to calculate the volume associated with each bead<sup>b</sup>.

#### Voronoi Volume and Deformation Level

Figure 2 shows the effect of the deformation on the Voronoi volume distribution. Increasing the deformation will increase almost homogeneously the free volume until cavitation takes place. During and after cavitation, the Voronoi volume distribution exhibits a significant tail representing the beads belonging to cavity walls. Note that after cavitation, the distribution relaxes to a narrower shape. Therefore, the cavitation process can be seen as an event, which *localizes* or *precipitates* the excess of free volume introduced by deformation.

#### Voronoi Volume and Bead Functionality

Figure 3 compares the mean Voronoi volume evolution of both regular beads and chain ends. It can be seen that chain ends exhibit a larger Voronoi volume, which is not surprising since, by construction, covalent and Lennard-Jones bonds have their energy minimum at  $0.96\sigma$  and  $1.12\sigma$ , respectively. Note that when cavitation occurs, the mean Voronoi volume of chain ends becomes very noisy due to statistical limitations. The insets of Figure 3 show that the Voronoi volume distributions have a Gaussian shape,

<sup>b</sup> See <http://math.lbl.gov/voro++/> and ref.<sup>[22]</sup>, where a very early version of this code was used.

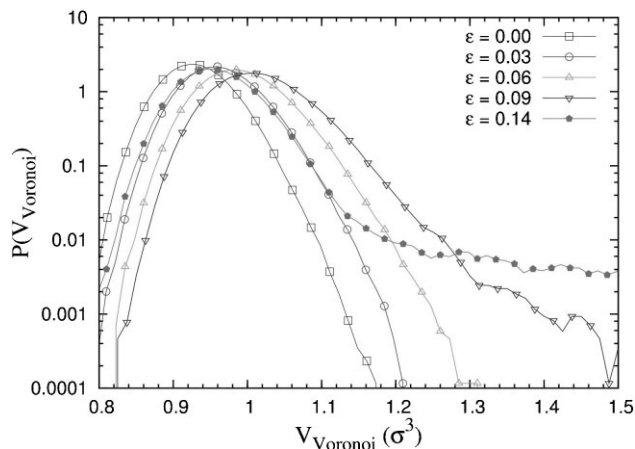


Figure 2. Voronoi volume distributions of configurations extracted over the deformation trajectory. Cavitation can be clearly seen in the tail of distribution. After cavitation, the distribution reverts to a narrower shape.

which shows the presence of low Voronoi volumes (much lower than the volume of an ideal disordered configuration). This calls into question the very concept of free volume, which is defined as that part of the atomic volume that can be redistributed throughout the system without change in energy,<sup>[23,24]</sup> i.e., the volume of an ideal disordered configuration. These points of extremely low volume could be related to the *constriction points* introduced by Stachurski<sup>[25]</sup> and, to a larger extent, to the *quasi-point defects* of Perez,<sup>[1]</sup> which represent points of high fluctuation of free energy.

#### Voronoi Volume and NAD

Within the free volume approach, deformation induced relaxations are supposed to be correlated with the available

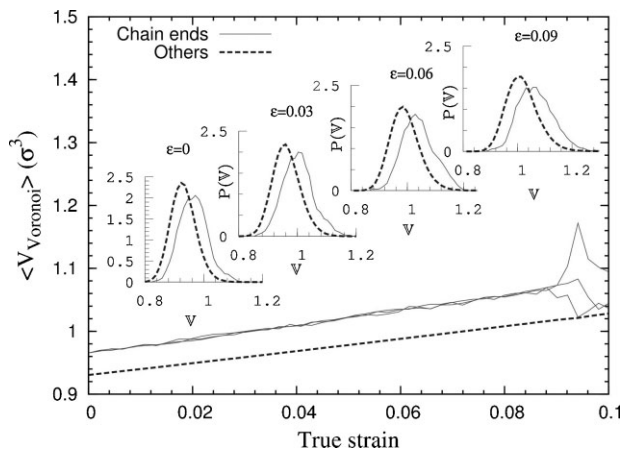


Figure 3. Evolution of the mean Voronoi volume of chain ends and other beads. Inset: Voronoi volume distributions during the course of deformation. No correlation can be observed between chain ends and Voronoi volume variation during tensile test.

free volume. Zones of larger free volume will therefore deform, changing the potential energy landscape and providing more free volume to zones of initially larger free volume. This explanation is often proposed to describe the formation of mechanical instabilities such as cavitation or shear bands. Motivated by these ideas, the search for a relationship between the magnitude of the NAD and the Voronoi volume becomes relevant.

Figure 4 shows a scatter plot obtained during deformation, where the magnitude of the NAD and the Voronoi volume were taken as variables. This scatter plot does not show a clear tendency for a correlation between NAD and Voronoi volume. Free volume represents the potential space for motion but it can not be seen as being a causal factor of the NAD and cavitation. The “cavity cluster” beads are also shown in this plot. In both cases, the points are distributed randomly and no noticeable trend was found, except during cavitation, where these beads exhibit larger NAD and slightly larger Voronoi volume. This analysis (not shown in this paper) was performed for several other temperatures ( $T=0.01$  and  $0.1$ ) and no correlation was found under these conditions either. Note that before cavitation, the magnitude of NAD remains much less than

the typical interatomic distance; in other words, the deformation is mostly affine.

### Stress Fluctuations

The local stress on any given bead can be obtained by dividing the classical expression of the virial stress by the Voronoi volume  $V_m$  of atom  $m$ ,<sup>[26]</sup>

$$\sigma_{ij}^m = -\frac{1}{2V_m} \left( m_m v_i^m v_j^m + \sum_{n \neq m} r_i^{mn} f_j^{mn} \right) \quad (2)$$

where  $v_i^m$  is the velocity  $i$ th component of atom  $m$ ;  $f_i^{mn}$  and  $r_i^{mn}$  are the  $i$ th component of force and distance between two interacting atoms  $m$  and  $n$ , respectively. The first term of this equation represent the kinetic contribution and the second one is the Cauchy stress. The hydrostatic stress  $S_{\text{hyd}}$  was calculated by computing the trace of the stress tensor,  $S_{\text{hyd}} = -(\sigma_{11} + \sigma_{22} + \sigma_{33})/3$

Figure 5 compares the distributions of hydrostatic stresses at several strains during deformation. In the initial nondeformed configuration, the distribution shows

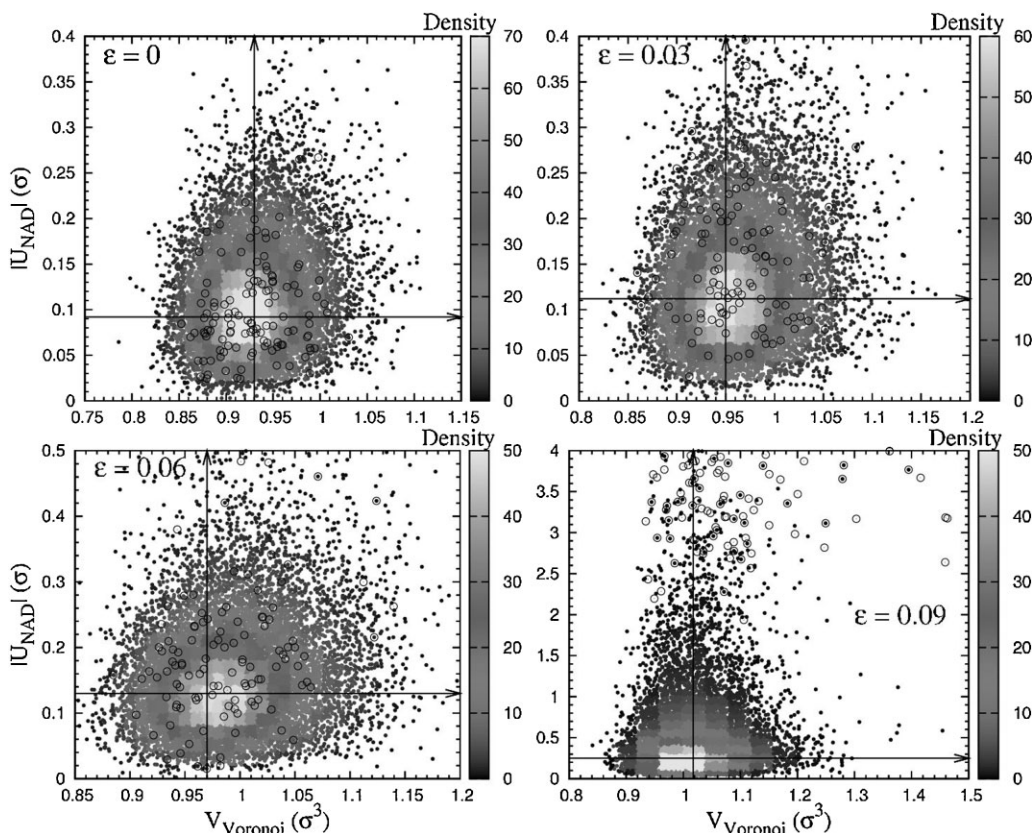


Figure 4. Non-affine displacement (NAD) magnitude of beads plotted against their Voronoi volume at several strains  $\varepsilon = 0, 0.03, 0.06,$  and  $0.09$  (cavitation). Arrows describe the higher density value of each variable. No correlation was found between these variables for all strains. “Cavity cluster beads” are marked by the symbol  $\circ$ : no remarkable trend can be distinguished, except during cavitation, where they exhibit larger NAD and slightly larger Voronoi volume.

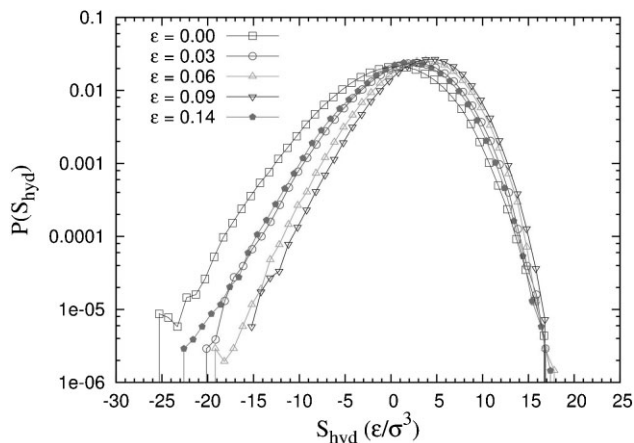


Figure 5. Distribution of hydrostatic stress at different deformation levels. The distribution narrows until the cavity opens, then broadens again.

an exponential tail toward negative values. As the deformation increases, the negative values of the hydrostatic stress are progressively relaxed, so that the distribution narrows and becomes more symmetrical just before cavitation takes place. These results are consistent with

those of ref.<sup>[26]</sup> After the cavitation has occurred, large negative values of the stress are again obtained, since the average free space is decreased as shown previously in Figure 2.

In order to investigate the correlation between NAD and the atomic hydrostatic stress, a scatter plot of these quantities is displayed in Figure 6. Apparently, there is no direct trend for a correlation between NAD and the hydrostatic stress at the scale of individual beads. The hydrostatic stress was also evaluated by considering each contribution separately (pair, bonded) at several strains, and again no correlations were found. When specific beads (chain ends and cavity cluster) values are selected in these scatter plots, the corresponding points appear to be a randomly chosen subset of the total sample. This absence of correlation may appear surprising, as the presence of a high local stress is often expected to result in plastic deformation. Note however that this result is consistent with a recent study<sup>[26]</sup> which showed no correlation between atomic stresses and shear yielding in polymers. In an analogous way, a previous study on sheared glasses<sup>[27]</sup> also failed to find a direct correlation between local stresses and the relevant local plastic deformation (shear transformations in that case).

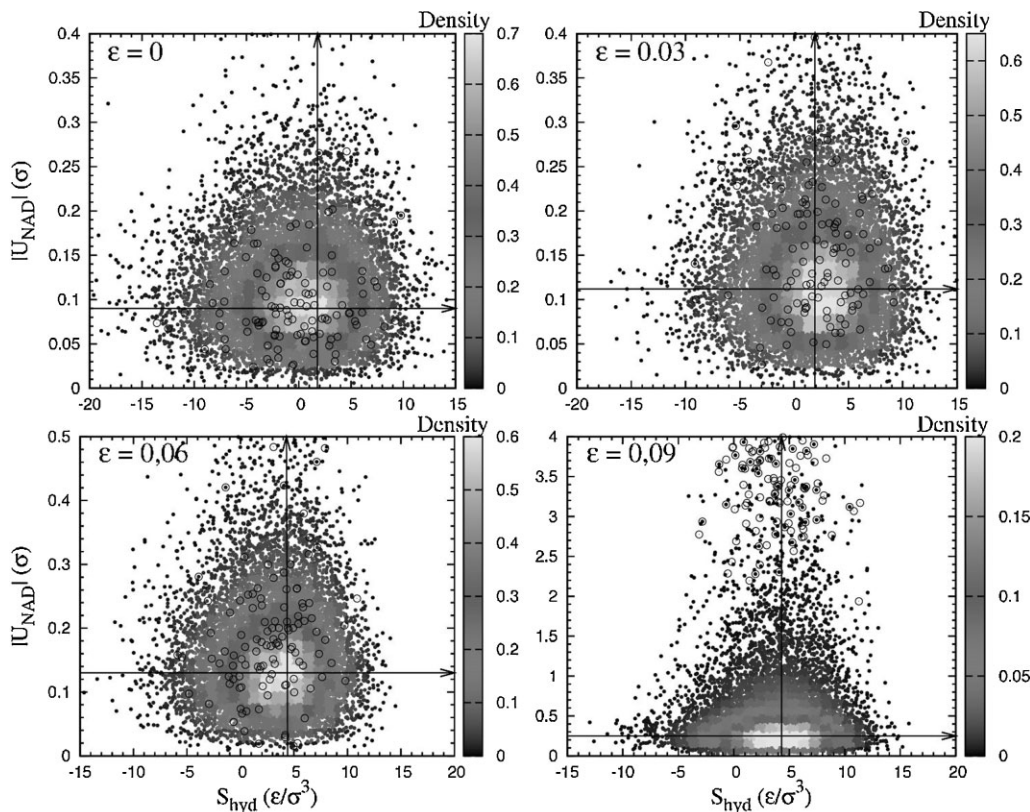


Figure 6. Scatter plot of the NAD against hydrostatic stress shown at the same deformation as in Figure 4. No clear trend for a correlation can be established. The values corresponding to the beads that surround the cavity labeled by the symbol  $\circ$  are randomly dispersed, thus preventing one to identify any specific correlation for these beads.

It may be, however, that a more coarse grained characterization is necessary to identify such correlations, and that the cavitation events are the result of a local heterogeneity that extends beyond the scale of individual beads. In order to assess this hypothesis, we describe briefly in the next section studies performed on density fields defined at a more coarse grained scale.

### Coarse-Grained Densities

The opening of a cavity under strain can be seen as a collective event, that involves at least those atoms that will form the cavity “skin” at the end of the process. The corresponding mechanical instability may therefore be the result of some density anomaly that extends over a region larger than a single atom size or Voronoi cell. We therefore have also explored the properties of our polymer system on such a coarse grained scale by defining continuous fields from the atomic positions. Various possibilities are available for such a coarse-graining procedure;<sup>[15,28,29]</sup> here we choose the simplest one, which consists in computing the densities on a regular grid by assigning to each grid node the atoms that belong to a fixed “voxel” volume around this node. The voxel size is taken in the range  $5\sigma$ – $7\sigma$ , which was shown in similar studies<sup>[14,26,30]</sup> to permit a good description in terms of continuous fields (with about 120 monomers per voxel) while preserving the locality and possible spatial heterogeneity of the variables under consideration.

We have attempted to coarse grain and to correlate with the appearance of cavities two of the densities examined previously at the atomic level, namely the density of chain ends and the density of monomers. The local density field is defined as:

$$\rho_i = \frac{n_i}{\sum_j V_i^j} \quad (3)$$

where  $n_i$  is the number of beads within a voxel  $i$ , and  $V_i^j$  is the Voronoi volume of the bead  $j$  that is included in the voxel  $i$ . Figure 7(a) shows the evolution of this local density with strain, and compares the average value with the value observed in the vicinity of the cavity.

These data show that the local density in the vicinity of the cavity follows the mean value until a deformation of  $\varepsilon = 0.06$ . Although cavitation does not occur until  $\varepsilon = 0.09$ , the local volume begins to decrease earlier (see inset). This observed trend can be interpreted by the fact that cavitation starts earlier than the drop of stress in the stress/strain-curve. This “pre-cavitation” behavior can be interpreted as resulting from a dynamical equilibrium between the elastic energy and the free surface energy of cavity with relatively small radius. This situation remains stable until the cavity reaches a critical radius (roughly estimated  $2\sigma$ ), beyond which the size of the cavity increases rapidly. The spatial distribution of the local density at  $\varepsilon = 0.08$ , just before the opening of the cavity is shown in part (b) of Figure 7. The lowest density spots are far from the expected position of the cavity, but a low density can be noticed in the cavity vicinity. In general, we have checked that a systematic decrease in density prior to cavitation is specific of the points that are located in the vicinity of the emerging cavity. Other points may display fluctuations in their values of the density, but these fluctuations remain uncorrelated with cavitation events. After the cavity nucleation, the low density regions that did not form cavities release their excess free volume introduced by the triaxial deformation condition. Therefore, the local density of such regions return to values similar to regions that are not involved in the cavitation. In conclusion, local loss of density should be seen rather as a consequence than as a cause of cavity nucleation.

As was mentioned above (in the Section ‘Voronoi Volume Fluctuations’), the free volume was found to be correlated with the bead connectivity. Chain ends exhibit a higher Voronoi volume compared to other monomers, and a lower density of beads could be expected where a higher density

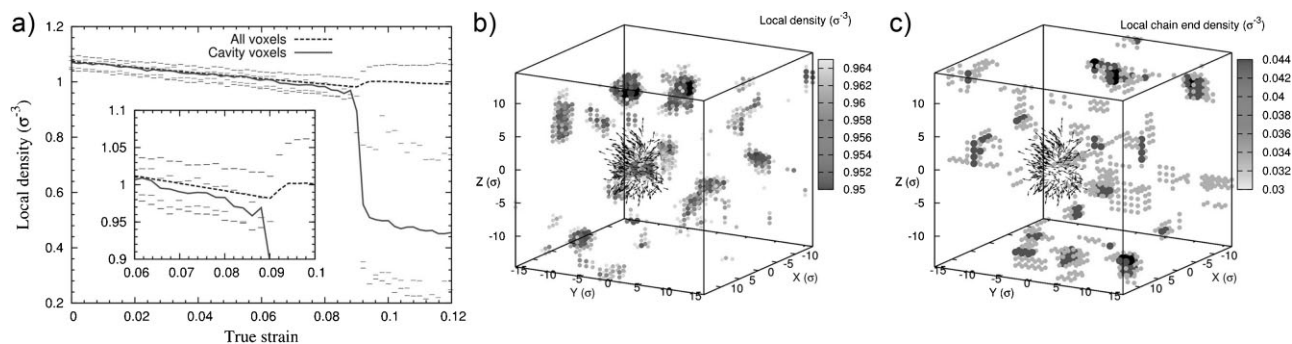


**Figure 7.** Evolution of mean local density calculated within cubic bins of size  $5 \times 5 \times 5\sigma^3$ . The average of the overall voxels (dashed line) is compared with the average of voxels that are associated with the cavity cluster beads (solid line). Symbols (-) denote the upper and lower values for each curve. The spatial distribution of local density taken at  $\varepsilon = 0.08$  is shown in (b) and the corresponding map of chain end density in (c). The arrows describe the NAD of the “cavity cluster beads.” The dark spots identify (b) the low-density vicinities and (c) the high-chain-end density.

of chain ends is present. We therefore define a local density of chain ends  $\rho^{\text{C.E.}}$  as

$$\rho_i^{\text{C.E.}} = \frac{n_i^{\text{C.E.}}}{V_i} \quad (4)$$

where  $n_i^{\text{C.E.}}$  is the number of chain ends within a voxel  $i$ , and  $V_i$  is the volume of the voxel. Figure 7(c) shows that, at this level of coarse-graining, the spatial distribution of chain ends is uncorrelated with the local density of beads and also with the cavity position. This indicates that the modification of the packing density by the presence of chain ends is insignificant. Summarizing, the coarse grained density of beads exhibits limited success as a predictor for cavity formation, as its evolution can be correlated with the formation of a cavity only shortly before the event actually takes place. The coarse grained density of chain ends, on the other hand, does not correlate well with the total density or with cavitation.

### Local Mechanical Properties

Our last attempt to identify a microstructural predictor for cavitation events is inspired by previous work on simple glassy systems under shear deformation, in which a low value of the shear moduli was identified as a good indicator for the occurrence of the relevant local plastic events.<sup>[14,15]</sup> Here, the relevant events involve a local dilatation of the material which eventually gives rise to a cavity, and points to the local bulk modulus as a possible predictor.

Local heterogeneity in the elastic properties of glasses is now a well documented feature, with a number of studies having shown that the moduli defined at intermediate scales (of the order of ten atomic sizes) are those of an isotropic but heterogeneous material. At such scales, a typical glassy sample can be described as consisting of coexisting “hard” and “soft” regions. This behavior is independent of the precise method which is used to define the coarse grained elastic constant, which may involve either the use of statistical mechanical formulas at a local scale,<sup>[13,14]</sup> or exploiting the linear relationship between coarse grained stress and strain field.<sup>[15]</sup> Here, we present results for the local bulk modulus obtained from a third approach, originally introduced by Sollich and Barra,<sup>[31]</sup> which has the advantage of being easily implemented at a reduced computational cost. The method can be summarized as follows: one first defines a coarse-graining volume as a fictive shape that encapsulates a number of beads. The shape was chosen spherical in order to reduce any potential boundary effects, and the radius equal to 3.5 particle diameters, consistent with the typical coarse-graining scales used in other methods.<sup>[14,15]</sup> The entire sample is then deformed affinely (in this case using a uniform dilation

of all bead coordinates). After this homogeneous deformation, all beads are kept frozen, except those contained in the coarse-graining volume which are allowed to fluctuate in a constant volume, constant temperature MD trajectory (here, we perform a trajectory at a rather low temperature,  $T = 0.01$ ). The increase in the hydrostatic stress  $S_{\text{hyd}}^m$  within the spherical volume  $m$  is obtained from the virial stress formula, and the local modulus  $K^m$  can be defined by dividing this stress by the imposed increase in volumetric strain  $\mathcal{V}^m$ :

$$K^m = \frac{d(S_{\text{hyd}}^m)}{\mathcal{V}^m} \quad (5)$$

In order to improve the accuracy on  $K^m$ , it has then been averaged over a dozen expansion tests within the domain  $0 < \mathcal{V}^m < 10^{-5}$ . A sequence of deformation (isotropic expansion) and relaxation steps is applied over the sample, and the gauge volume  $V^m$  and  $S_{\text{hyd}}^m$  are measured after each step. The expansion is limited to a very low deformation amount since the measurement is restricted to the elastic regime only. Substituting  $\mathcal{V}^m$  by its definition  $dV^m/V^m$  leads to another form of Equation 5:

$$K^m \cdot \frac{dV^m}{V^m} = d(S_{\text{hyd}}^m) \quad (6)$$

or equivalently

$$K^m \ln(V^m)|_0^t = S_{\text{hyd}}^m|_0^t \quad (7)$$

where  $V^m$  and  $S_{\text{hyd}}^m$  are integrated along the deformation trajectory from 0 to  $t$ . This method allows us to obtain an accurate determination of  $K^m$  in the linear regime by fitting the data obtained for  $S_{\text{hyd}}^m = f(\ln(V^m))$ . This

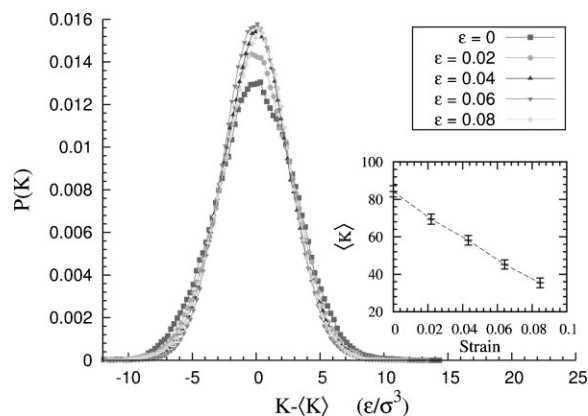


Figure 8. Density distribution of local bulk modulus for the same specimen at several deformation levels. Distributions are shifted by their mean values. The inset shows the evolution of the mean values. Error bars are deduced from the standard deviation.

procedure was applied along each tensile deformation trajectory, for positions of the center of the coarse-graining volume distributed on a regular grid.

Figure 8 compares the statistical distributions of the local bulk modulus at different strain levels. The plotted distributions are shifted by their mean values to facilitate

comparison of their shapes. Curves remain symmetrical and Gaussian, whatever the applied strain before cavitation. As the deformation increases, the distribution will become slightly narrower. This behavior is consistent with the trend described in the previous sections, that the polymeric system tends to homogenize its local stress under

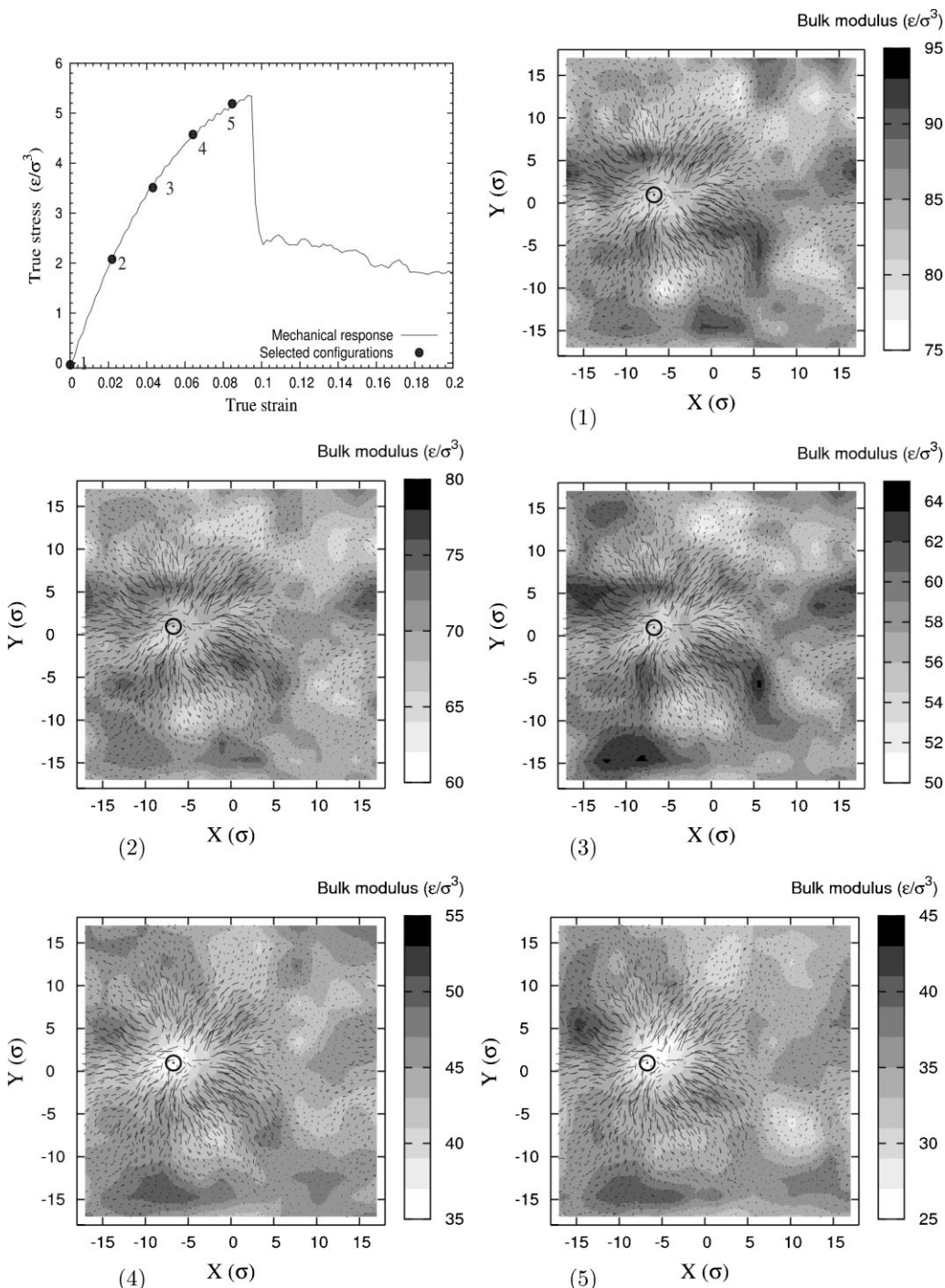


Figure 9. XY Layers taken from the spatial distribution of the bulk modulus (tensile direction is Z in this case). The Z coordinate of all layers corresponds to the cavity position. Every layer is indexed (bottom left corner) referring to its position in the stress/strain curve on the upper left. These maps are superimposed with the NAD at  $\epsilon = 0.09$  that shows the formation of the cavity.

an applied deformation. The mean value of the local bulk modulus (see inset) decreases continuously as the deformation increases and more free volume is introduced in the system.

In order to investigate the spatial distribution of the local bulk modulus, two-dimensional slices in a plane perpendicular to the tensile direction were taken at the level at which the cavity is observed. Figure 9 shows a sequence of such bulk modulus cartographies that are captured along the deformation trajectory. Each slice corresponds to one of the blue markers on the stress strain curve (first plot in Figure 9). The nonaffine vectors describing the formation of a cavity are also plotted on each map. As can be seen, the local bulk modulus fluctuates between high and low values at each strain, and the position at which the cavity appears corresponds to one of the low bulk modulus sites identified in the starting configuration. When the deformation increases, an extremely low value of bulk modulus appears in the expected position of cavity, as in slices (4) and (5). The lower value indicated here is not only a local minimum in the plane of the figure, but instead corresponds to the lowest value for the entire sample.

In the light of this strong correlation between NAD and elastic modulus, the cavitation process in glassy polymers

can be described in the following manner: the polymeric system exhibits some fluctuations in the local elastic bulk modulus. As the deformation progresses, the statistical distribution of the bulk modulus changes: the mean value decreases, but the contrast of spatial distribution is conserved. At relatively high strain, one of the zones that initially displayed a low bulk modulus will reach an anomalous value, resulting in a favorable location for the subsequent growth of a cavity.

We will now investigate whether this behavior should be described as deterministic (the cavity systematically forms in a particular zone) or rather statistical (the cavity forms randomly in one of the zones with a low modulus) process. To this end, the same system was subjected to three tensile tests with different tensile directions  $x$ ,  $y$ , and  $z$ . The positions at which cavitation takes place were recorded and compared after each test.

Figure 10(a) shows that, for the same initial configuration, cavities nucleate in different zones. The same behavior was also found for several systems with different temperatures. The cavities systematically nucleate in zones that are characterized by a low modulus in the initial state; however, the specific site at which it is observed depends on the deformation path and on the tensile direction.

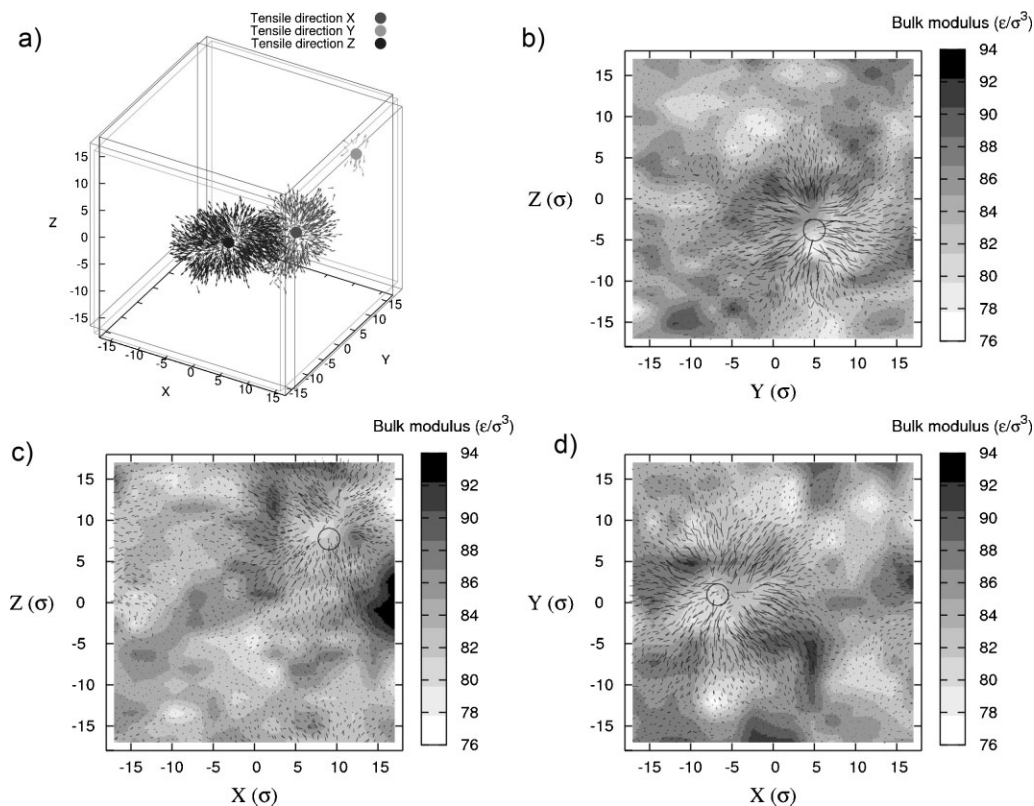


Figure 10. (a) Positions of cavities in a single sample after tensile tests with different straining directions. The vectors describing the formation of a cavity are superimposed with the corresponding map of local elastic bulk modulus imaged in the initial, nondeformed, configuration. Slices (b), (c), and (d) are located in the corresponding position of the cavity nucleation and they are perpendicular to the tensile directions  $X$ ,  $Y$ , and  $Z$ , respectively.

## Conclusion

In this work, the relationship between a cavitation event in a glassy polymer undergoing a tensile test and the local properties has been investigated with MD simulations. Several properties have been analyzed at two different length scales: the elementary scale of the monomer, and a coarse-graining scale of 5–10 particle diameters. Independent of the scale under consideration, we find that the density of monomers or the density of chain ends do not correlate with the subsequent appearance of a cavity. In contrast, the bulk modulus in the nonstrained configuration displays fluctuations that can be directly related, in a statistical sense, to the appearance of a cavity at large deformations. Note that very similar conclusions with regard to the importance of local elastic moduli for cavitation were reached by Toepferweine and de Pablo in a recent study that considered both homopolymers and composite systems.<sup>[32]</sup> This situation resembles those observed in glassy materials under volume conserving shear, where a weak shear modulus indicates a tendency for plastic rearrangement.

**Acknowledgements:** Computational support was provided by the Federation Lyonnaise de Calcul Haute Performance and GENCI/CINES. The financial support from the ANR project Nanomeca is acknowledged. Part of the simulations were carried out using the LAMMPS molecular dynamics software (<http://lammmps.sandia.gov>).

Received: January 19, 2011; Revised: May 11, 2011; Published online: August 23, 2011; DOI: 10.1002/mats.201100006

**Keywords:** cavitation; computational modeling; mechanical properties; molecular dynamics simulations; plasticity

- [1] J. Perez, *Physics and Mechanics of Amorphous Polymers*, Balkema, Rotterdam 1998.
- [2] S. Humbert, O. Lame, J. M. Chenal, C. Rochas, G. Vigier, *Macromolecules* 2010, 43, 7212.

- [3] K. P. Herrmann, V. G. Oshmyan, *Int. J. Solids Struct.* 2002, 39, 3079.
- [4] A. S. Argon, J. G. Hannoosh, *Philos. Mag.* 1977, 36, 1195.
- [5] R. Estevez, M. G. A. Tijssens, E. Van der Giessen, *J. Mech. Phys. Solids* 2000, 48, 2585.
- [6] A. N. Gent, *J. Mater. Sci.* 1970, 5, 925.
- [7] S. S. Sternstein, L. Ongchin, *Polym. Prepr.* 1969, 10, 1117.
- [8] P. B. Bowden, R. J. Oxborough, *Philos. Mag.* 1973, 28, 547.
- [9] J. Rottler, M. O. Robbins, *Phys. Rev. E* 2001, 64, 051801; *Phys. Rev. E* 2003, 68, 011801.
- [10] B. Sixou, *Mol. Simul.* 2007, 33, 965.
- [11] D. K. Mahajan, B. Singh, S. Basu, *Phys. Rev. E* 2010, 82, 011803.
- [12] K. Yoshimoto, G. J. Papakonstantopoulos, P. F. Lutesko, J. J. de Pablo, *Phys. Rev. B* 2005, 71, 184108.
- [13] K. Yoshimoto, T. S. Jain, K. Van Korkum, P. F. Nealey, J. J. de Pablo, *Phys. Rev. Lett.* 2004, 93, 175501.
- [14] G. J. Papakonstantopoulos, R. Riggleman, J.-L. Barrat, J. J. de Pablo, *Phys. Rev. E* 2008, 77, 041502.
- [15] M. Tsamados, A. Tanguy, C. Goldenberg, J. L. Barrat, *Phys. Rev. E* 2009, 80, 026112.
- [16] K. Kremer, G. S. Grest, *J. Chem. Phys.* 1990, 92, 5057.
- [17] M. Perez, O. Lame, F. Leonforte, J. L. Barrat, *J. Chem. Phys.* 2008, 128, 234904.
- [18] R. Auhl, R. Everaers, G. S. Grest, K. Kremer, S. J. Plimpton, *J. Chem. Phys.* 2003, 119, 12718.
- [19] A. Makke, M. Perez, O. Lame, J. L. Barrat, *J. Chem. Phys.* 2009, 131, 014904.
- [20] B. Schnell, *Ph. D. Thesis*, Université de Strasbourg 2006.
- [21] M. Tsamados, *Eur. Phys. J. E* 2010, 32, 165.
- [22] C. H. Rycroft, G. S. Grest, J. W. Landry, M. Z. Bazant, *Phys. Rev. E* 2006, 74, 021306.
- [23] D. Turnbull, M. Cohen, *J. Chem. Phys.* 1961, 34, 120.
- [24] D. Turnbull, M. Cohen, *J. Chem. Phys.* 1970, 52, 3038.
- [25] Z. H. Stachurski, *Polymer* 2003, 44, 6067.
- [26] D. MacNeill, J. Rottler, *Phys. Rev. E* 2010, 81, 011804.
- [27] M. Tsamados, A. Tanguy, F. Leonforte, J.-L. Barrat, *Eur. Phys. J. E* 2008, 26, 283.
- [28] I. Goldhirsch, C. Goldenberg, *Eur. Phys. J. E* 2002, 9, 245.
- [29] F. A. Detcheverry, D. Q. Pike, P. F. Nealey, M. Müller, J. J. de Pablo, *Faraday Discuss.* 2010, 144, 111.
- [30] J. P. Wittmer, A. Tanguy, J. L. Barrat, L. Lewis, *Europhys. Lett.* 2002, 57, 423.
- [31] P. Sollich, A. Barra, in preparation.
- [32] G. N. Toepferweine, J. J. de Pablo, *Macromolecules* 2011, 44, 5498.